Strength Design Criteria for Steel Beam-Columns with Fire-Induced Thermal Gradients

MAHMUD M.S. DWAIKAT and VENKATESH K.R. KODUR

ABSTRACT

When exposed to fire, restrained steel members develop significant internal forces, and these forces transform their behavior from beams or columns to that of beam-columns. The current provisions for fire-resistance assessment of such beam-columns through *P-M* interaction equations are an extension to the ambient interaction equations. These fire design equations take into consideration the reduction in the capacity arising from temperature-induced degradation of strength and stiffness properties but do not take into account the effect of other critical factors, such as thermal gradient, end restraints and realistic fire scenarios (with cooling phase). In this study, the different fire design equations for steel beam-columns are compared against results from nonlinear finite element simulations. Results from the analysis show that fire-induced thermal gradient leads to not only a reduction in the *P-M* diagrams, but also a noticeable distortion in the shape of the *P-M* diagrams. Therefore, modifications are proposed to the current design interaction equations for steel beam-columns at elevated temperatures. The modified *P-M* design equations are validated against results from fire tests and from finite element analysis and then illustrated through a design example. The proposed approach requires minimum computational effort and provides better assessment of beam-columns under fire when compared to current provisions.

Keywords: beam-columns, elevated temperatures, fire, interaction equations.

INTRODUCTION

The current approach of computing *P-M* curves and related fire resistance of steel structural members is based on the assumption that a uniform temperature prevails across the depth of the section (AISC, 2005; EC3, 2005). However, in practice a steel beam or column might be exposed to fire from one, two or three sides, such as in beams supporting slabs or columns in the perimeter of a framed building. In such scenarios, the beams and columns are likely to develop nonuniform thermal gradients across the depth of the section, and this will significantly alter the shape of the *P-M* capacity curves (Dwaikat and Kodur, 2009).

The effect of thermal gradients on the load-carrying capacity of beam-columns has received little attention in the literature. The plastic *P-M* interaction curves for steel sections under fire conditions were studied by Ma and Liew (2004) by simulating inelastic response of beam-columns in steel frames. However, the authors used average steel temperature and did not account for the effect of thermal gradients. The influence of thermal gradients on the plastic moment capacity was investigated by Burgess et al. (1990) by discretizing the section into strips and then numerically integrating the sectional stresses at full yield. However, the effect of axial force on the plastic moment capacity was not considered in the analysis.

Takagi and Deierlein (2007) assessed the sensibility of extending the room-temperature Eurocode 3 and AISC design equations to fire design through finite element analysis. In their study, they found that the AISC design equations are nonconservative when applied under fire conditions. Takagi and Deierlein proposed adjustments to room-temperature moment and axial capacities (M_{cr} and P_{cr}) of steel members for use at elevated temperature. Further, they recommended the use of the modified M_{cr} and P_{cr} into the AISC *P-M* interaction equations at elevated temperature, and these modified equations are being implemented in the 2010 AISC *Specification for Structural Steel Buildings*. However, the proposed adjustments do not take into consideration the influence of thermal gradients on M_{cr}, P_{cr} or the *P-M* interaction equation.

The underlying mechanics of the distortion of *P-M* diagrams that is induced by thermal gradients was studied by Garlock and Quiel (2007, 2008). These studies showed that a thermal gradient in a steel section causes the center of stiffness, *CS*, of the cross section to migrate toward the cooler (stiffer) regions and away from the heated (softer) regions. This migration of the center of stiffness generates an eccentricity, *e*, between the geometric center, *CG*, and the center of stiffness of the cross section. As a result of

Mahmud M.S. Dwaikat, Ph.D. candidate, Civil and Environmental Engineering Department, Michigan State University, East Lansing, MI. E-mail: dwaikat1@egr.msu.edu

Venkatesh K.R. Kodur, Professor, Civil and Environmental Engineering Department, Michigan State University, East Lansing, MI. E-mail: kodur@egr.msu.edu

this eccentricity, bending moment is generated because the axial force will now act eccentrically with respect to the new center of stiffness of the section. This generated bending moment may counteract the bending moment that results due to thermal bowing. Therefore, this migration of center of stiffness causes a distortion in the plastic *P-M* interactive diagram (Dwaikat and Kodur, 2009; Garlock and Quiel, 2007, 2008).

Based on these studies, Garlock and Quiel (2008) proposed a numerical procedure to compute the resulting distorted *P-M* diagrams for an I-shaped cross section subjected to any thermal gradient of any shape. The proposed method requires intensive use of numerical programs, such as MATLAB, or spreadsheets. For example, lengthy algorithms are required to compute the lumped temperature in each steel plate of the section to numerically integrate the temperature-dependent ultimate stresses along the depth of the cross section. This makes the method laborious and not straightforward.

Further research by Dwaikat and Kodur (2009) on the influence of fire-induced thermal gradient on *P-M* diagrams has led to modifications to the current interaction *P-M* equations in codes and standards. However, the study by Dwaikat and Kodur (2009) was limited to rigid plastic failure modes (plastic *P-M* diagrams). In this study, an improved and simplified approach is presented for estimating the distorted *P-M* diagrams of I-shaped cross section induced by thermal gradients. The proposed approach accounts for plastic as well as second-order inelastic failure modes in steel beam-columns under fire conditions. While the idea of this paper is true for any kind of beam-column subjected to thermal gradient, the proposed equations are only valid for I-shaped cross sections subjected to thermal gradient in their strong direction. The proposed method utilizes simplifying assumptions for predicting the distorted *P-M* curves and does not require complex numerical integration of sectional ultimate stresses.

CURRENT FIRE PROVISIONS FOR BEAM-COLUMNS

AISC Approach

The 2005 AISC *Specification* recommends the use of ambient temperature design equations for fire design, but with temperature-reduced strength and stiffness steel properties (AISC, 2005). The design capacity of steel beam-columns in AISC is given in the form of an interaction relation between bending moment and the axial force:

$$c_1 \frac{P}{\phi P_{cr}} + c_2 \frac{M}{\phi M_{cr}} \leq 1.0 \tag{1}$$

where P and M are the applied axial force and bending moment, P_{cr} and M_{cr} are the critical axial force and bending moment capacities; $c_1 = 1$ and $c_2 = 8/9$ when $P/P_{cr} \geq 0.2$, but when $P/P_{cr} < 0.2$, $c_1 = 0.5$ and $c_2 = 1$.

The critical axial capacity (P_{cr}) is given as:

$$P_{cr}^{\text{AISC}} = \begin{cases} \left(0.658^{F_y(T)/F_e(T)}\right) P_y(T), & K\lambda \leq 4.71\sqrt{\dfrac{E_s(T)}{F_y(T)}} \\ 0.877 A_s F_e(T), & K\lambda > 4.71\sqrt{\dfrac{E_s(T)}{F_y(T)}} \end{cases} \tag{2}$$

where $\lambda = L/r_y$ is the slenderness ratio, K is the effective length factor, and r_y and A_s are the minimum radius of gyration and the cross sectional area of the column, respectively. $F_y(T)$ and $E_s(T)$ are the temperature-dependent yield strength and elastic modulus of steel, respectively. The plastic axial capacity, $P_y(T)$, is defined as $A_sF_y(T)$, and $F_e(T)$ is the temperature-dependent elastic Euler buckling stress given as:

$$F_e(T) = \frac{E_s(T)\pi^2}{(K\lambda)^2} \tag{3}$$

The critical bending moment capacity M_{cr} in Equation 1 is computed as:

$$M_{cr}^{\text{AISC}} = \left.\begin{cases} M_p(T), & \lambda \leq \lambda_p(T) \\ C_b\left(M_p(T) - \left(M_p(T) - S_xF_r(T)\right)\dfrac{\lambda-\lambda_p}{\lambda-\lambda_r}\right), & \lambda_p(T) < \lambda \leq \lambda_r(T) \\ C_bM_e(T), & \lambda > \lambda_r(T) \end{cases}\right\} \leq M_p(T) \tag{4}$$

In Equation 4, $F_r(T) = 0.7F_y(T)$ is the stress required to reach initial yielding when added to the residual stress. Here, Z_x and S_x are the plastic and elastic sectional moduli, respectively; $M_p(T)$ is the temperature-dependent plastic moment defined as $M_p(T) = F_y(T)Z_x$; C_b is a factor that accounts for the shape of the bending moment diagram, where $C_b = 1.14$ for uniformly loaded simply supported beam; and $M_e(T)$ is the temperature-dependent elastic lateral-torsional buckling moment:

$$M_e(T) = \frac{\pi}{L}\sqrt{E_s(T)I_yG_s(T)J + I_yC_w\left(\frac{\pi}{L}E_s(T)\right)^2} \tag{5}$$

The limiting slenderness ratios in Equation 4 are:

$$\lambda_p = 1.76\sqrt{E_s(T)/F_y(T)} \tag{6a}$$

$$\lambda_r(T) = \frac{\pi}{F_r(T)S_x}\sqrt{\frac{E_s(T)G_s(T)JA_s}{2}} \sqrt{1+\sqrt{1+4\frac{C_w}{I_y}\left(\frac{F_{cr}(T)S_x}{G_s(T)J}\right)^2}} \tag{6b}$$

where I_y, C_w and J are the second moment of area around the weak axis, the warping constant, and the torsional constant of the section, respectively, and $G_s(T)$ is the elastic shear modulus. In order to account for the second-order effect, the applied bending moment (M_o) is generally magnified by a factor β such that:

$$M = \beta_{\text{AISC}} \times M_o \tag{7}$$

where M is the second-order moment and M_o is the first-order elastic bending moment. The magnification factor β_{AISC} is defined as:

$$\beta_{\text{AISC}} = \frac{C_m}{1-P/P_e} \geq 1 \tag{8}$$

where C_m is a coefficient that accounts for the moment gradient on the beam-column and is given as:

$$C_m = 0.6 - 0.4(M_1/M_2) \tag{9}$$

Here, M_1 and M_2 are the smaller and larger moments, respectively, at the ends of the beam-column; M_1/M_2 is positive when the member is bent in reverse curvature but negative when bent in single curvature, and P_e is the elastic Euler axial buckling load, [$P_e = A_sF_e(T)$, with $K = 1.0$, unless the analysis indicates that a smaller value of K may be used].

The critical bending and axial compressive capacity equations according to the 2005 AISC *Specification* are plotted in Figures 1 and 2, respectively, as a function of slenderness ratio and for different temperatures.

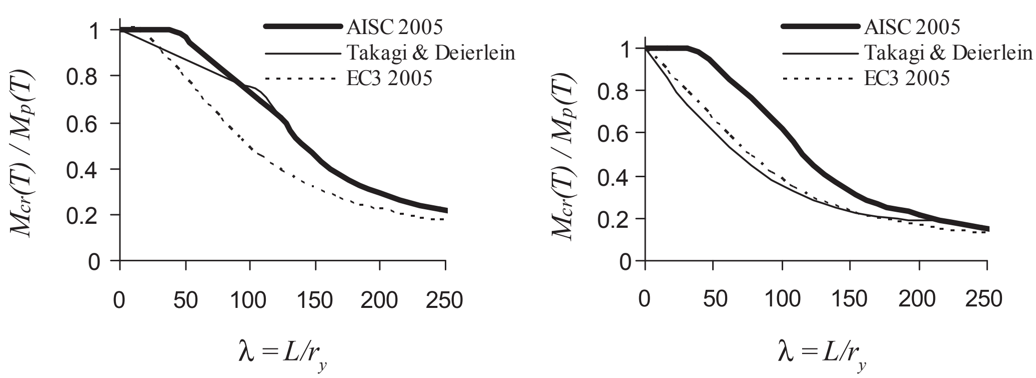

(a) *(b)*

Fig. 1. Critical moment capacity at elevated temperature for W-shapes: (a) T = 20 °C (68 °F); (b) T = 500 °C (932 °F).

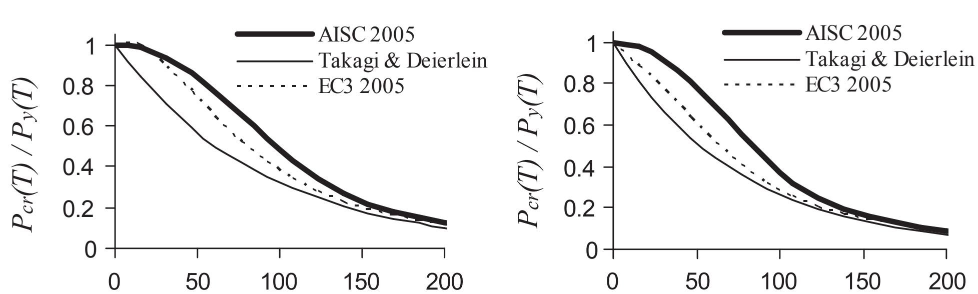

(a) *(b)*

Fig. 2. Critical axial capacity at elevated temperature for W-shapes: (a) T = 20 °C (68 °F); (b) T = 500 °C (932 °F).

Eurocode Approach

In the Eurocode 3 (EC3, 2005) the capacity of steel beam-columns under fire is assessed using an interaction equation similar to AISC (Equation 1), but with $c_1 = c_2 = 1$. The critical moment and axial capacities, M_{cr} and P_{cr} in Equation 1, have different definitions in EC3.

The critical axial capacity is defined in EC3 as:

$$P_{cr}^{\text{EC3}} = \chi_C(T)P_y(T) \tag{10}$$

where

$$\chi_C(\text{T}) = \frac{1}{\phi + \sqrt{\phi^2 - \bar{\lambda}^2}} \leq 1 \tag{11a}$$

$$\phi = \frac{1 + \alpha\bar{\lambda} + \bar{\lambda}^2}{2} \tag{11b}$$

$$\alpha = 10 / \sqrt{F_y(\text{in MPa})} \tag{11c}$$

$$\bar{\lambda} \quad \bar{\lambda} = \sqrt{F_y(T)/F_e(T)} \tag{11d}$$

The critical bending moment is defined in EC3 as:

$$M_{cr}^{\text{EC3}} = \chi_B(T)M_p(T) \tag{12}$$

where $\chi_B(T)$ accounts for reduction due to lateral torsional buckling and is computed similar to $\chi_C(T)$ but using normalized slenderness of $\bar{\lambda} = \sqrt{M_p(T)/M_e(T)}$.

The second-order effect factor β in Eurocode has a different form:

$$\beta_{\text{EC3}} = 1 - \mu\frac{P}{P_{cr}} \leq 1 \tag{13}$$

The factor μ is to account for lateral torsional buckling and is defined for compact sections as:

$$\mu = 0.15\bar{\lambda}\beta_M - 0.15 \leq 0.9 \tag{14}$$

where β_M is the equivalent uniform moment factor that depends on the shape of bending moment diagram. In case of uniform bending moment, $\beta_M = 0.7$.

The critical bending and axial compressive capacity equations according to Eurocode are plotted in Figures 1 and 2, respectively, as function of slenderness ratio and for different temperatures.

Takagi and Deierlein (T&D) Approach

Based on a comparison between the current design approaches and nonlinear finite element analysis, Takagi and Deierlein (2007) suggested modifications to the 2005 AISC *Specification* strength and stability design equations under fire conditions. The modifications included new expressions for critical moment and axial capacities (M_{cr} and P_{cr}); however, the same AISC *P-M* interaction equation (Equation 1) was maintained. It is worth mentioning that these proposed adjustments are based on uniform temperature distribution across the beam cross section.

According to Takagi and Deierlein, the critical axial capacity is given as:

$$P_{cr}^{\text{T\&D}} = \left[0.42^{\sqrt{F_y(T)/F_e(T)}}\right]P_y(T) \tag{15}$$

The critical moment capacity is given as:

$$M_{cr}^{\text{T\&D}} = \begin{cases} S_xF_{cr}(T) + \left[M_p(T) - S_xF_{cr}(T)\right]\left(1 - \dfrac{\lambda}{\lambda_r(T)}\right)^{C_X}, & \lambda \leq \lambda_r(T) \\ \dfrac{\pi}{L}\sqrt{E_s(T)I_yG_s(T)J + I_yC_w\left(\dfrac{\pi}{L}E_s(T)\right)^2}, & \lambda > \lambda_r(T) \end{cases} \leq M_p(T) \tag{16}$$

The equation for $\lambda_r(T)$ is the same as Equation 6b but using a different value of $F_r(T)$:

$$F_r(T) = k_p(T)F_y - k_y(T)F_{rs} \tag{17}$$

where $k_p(T)$ and $k_y(T)$ are the temperature-dependent reduction factors for proportionality limit and yield strength of steel, respectively, as specified by Eurocode 3 (2005); F_{rs} is the residual stress at ambient temperature and is specified in AISC (2005) as 69 MPa; $C_x = 0.6 - T/250$, where T is steel uniform temperature in degrees Celsius, and C_x must always be less than 3.

Figures 1 and 2 compare AISC, Eurocode 3 and Takagi and Deierlein design curves for bending and axial compressive capacity of steel beams at elevated temperature as a function of slenderness ratio λ. The curves shown in Figures 1 and 2 are adapted from Takagi and Deierlein (2007) and form a basis for provisions in the 2010 AISC *Specification*. The bending and axial capacities as a function of steel temperature [$M_{cr}(T)$ and $P_{cr}(T)$] are normalized with respect to the plastic bending and axial capacities at elevated temperature [$M_p(T)$ and $P_y(T)$].

Based on the trends in Figures 1 and 2, the Eurocode approach is the most conservative under fire conditions [for $M_{cr}(T)$], while the 2005 AISC equations are the least conservative. Further, while the reduction in M_{cr} and P_{cr} according to Eurocode and 2005 AISC equations starts after a certain slenderness ratio, the reduction in M_{cr} and P_{cr} according to the T&D approach starts immediately for nonzero slenderness (see Figure 1). The results of nonlinear finite element analysis carried out by Takagi and Deierlein showed that the reduction in M_{cr} indeed starts immediately for nonzero slenderness and that plastic bending capacity is only achieved for fully braced members under fire conditions. Based on these conclusions, Takagi and Deierlein proposed modified equations such that reduction in M_{cr} occurs immediately for nonzero slenderness beams.

INFLUENCE OF THERMAL GRADIENT

In all of the previously mentioned approaches, effect of fire-induced thermal gradient is accounted for by applying temperature-dependent reduction factors to room-temperature steel strength properties. The Eurocode (EC3, 2005) accounts for thermal gradient through applying numerical integrals for the axial and moment plastic capacities of the section only; that is:

$$P_y(T) = F_y \int k_y(T_i)dA = F_y \sum A_i k_y(T_i) \tag{18}$$

$$M_p(T) = F_y \int k_y(T_i)z_i dA = F_y \sum z_i A_i k_y(T_i) \tag{19}$$

The Eurocode procedure accounts for strength variation due to thermal gradient across the steel section; however, the stiffness variation due to thermal gradient across the section is not captured by this approach. In the AISC and T&D proposed equations, the influence of thermal gradient is not treated at all.

Thermal gradient can have a major influence on the shape of the interaction *P-M* Equation 1. Due to uneven heat distribution in the section, the center of stiffness of the section shifts from its original position. Because of the gradient-induced shift in the center of stiffness, the axial force will act eccentrically on the section and thus generate bending moment. This issue of shifting center of stiffness, which can have a major influence on beam-column response, is not treated in most design standards.

Also, thermal gradient has a direct influence on the second-order bending moments acting on the beam-column. This is due to the fact that thermal gradient leads to thermal bowing of the beam-column, and this increases the bending moment induced due to the *P*-Δ effect. Therefore, if the beam-column is not fully braced, the moment due to the *P*-Δ effect, which results from the thermal bowing, can be quite significant and thus causes premature strength failure of the beam-column. In all codes and standards, this critical influence of thermal gradient on the *P*-Δ effect is not treated explicitly and is left to the designer to quantify. The quantification of the *P*-Δ effect resulting from the thermal gradient often requires intensive use of complex finite element modeling.

PROPOSED MODIFICATIONS

Modifications to the design equations specified in codes and standards are proposed in order to account for the influence of thermal gradient on the capacity of steel beam-columns. The first modification is at the sectional level and is related to the distortion of the *P-M* diagram, which occurs as a result of the gradient-induced shift between center of stiffness and center of geometry of the cross section. The second modification is at the global (member) level and is related to the increased second-order effect (*P*-Δ effect) that results from thermal bowing caused by fire-induced thermal gradients. Both modifications will lead to change in the applied bending moment on the beam-column.

In a previous study by the authors (Dwaikat and Kodur, 2009), it was shown that the distortion of the *P-M* diagrams for beam-columns subjected to thermal gradient in the weak direction is negligible. Also, because the beam-columns are generally braced in their weak direction, the *P*-Δ effect (that would result from thermal bowing) can be neglected too. Thus, no modifications are required for the *P-M* diagrams in the weak direction of the beam-columns. Herein, modifications are proposed for the *P-M* diagrams for beam-columns subjected to thermal gradient across their strong (generally unbraced) axis.

When a beam-column is exposed to fire from one, two or three sides only, as shown in Figure 3a, thermal gradient (ΔT) develops across the cross section, and this gradient causes a migration of the center of stiffness from the hotter side to the cooler side of the cross section. This migration of center of stiffness leads to a corresponding distortion of the *P-M* diagrams of the beam-column. The basic features of the distorted plastic *P-M* diagrams for a W-section with thermal gradient in the strong direction are compared to the case of a uniform temperature in Figure 3b. The figure shows that the value of moment capacity under peak axial capacity (point A in Figure 3b) moves back and forth (to point A′ in Figure 3b) depending on the eccentricity e between center of stiffness, CS, and center of geometry, CG, that is caused by the thermal gradient in a W-section. The magnitude of the shift M_{TG} in the *P-M* capacity envelope (Figure 3b) is assumed to be numerically equal to the ultimate axial capacity $P_{u,Tave}$ of the section multiplied by the eccentricity e between the center of geometry, CG, and of the center of stiffness, CS, of the section as shown in Figure 3b. The ultimate capacity is computed based on the average temperature of the section:

$$M_{TG} = e \times P_{y,Tave} = e \times k_y(T_{s,Ave}) \times F_y \times A_s \tag{20}$$

To compute the eccentricity e between Y_{CS} and Y_{CG}, the reduction in the elastic modulus of steel is assumed to vary linearly across the depth of the section as shown in Figure 4. Each plate of the section is assumed to have a constant rate of reduction, k_E, in the elastic modulus, depending on its average temperature. The reduction in elastic modulus of the steel in the web is assumed to equal the average of the reductions of both the top (cool) and bottom (hot) flanges. With these assumptions, the eccentricity e between Y_{CG} and Y_{CS} across the strong axis can then be calculated as follows:

$$e = Y_{CS} - Y_{CG} = \frac{\sum A_i \times k_E(T_i) \times y_i}{\sum A_i \times k_E(T_i)} - \frac{d}{2} \tag{21}$$

$$e = \frac{b_F t_F k_E(T_{s,CF}) \times d + \left(\frac{k_E(T_{s,CF}) + k_E(T_{s,HF})}{2}\right) t_w d \times \frac{d}{2}}{b_F t_F k_E(T_{s,CF}) + \left(\frac{k_E(T_{s,CF}) + k_E(T_{s,HF})}{2}\right) t_w d + b_F t_F k_E(T_{s,HF})} - \frac{d}{2} \tag{22}$$

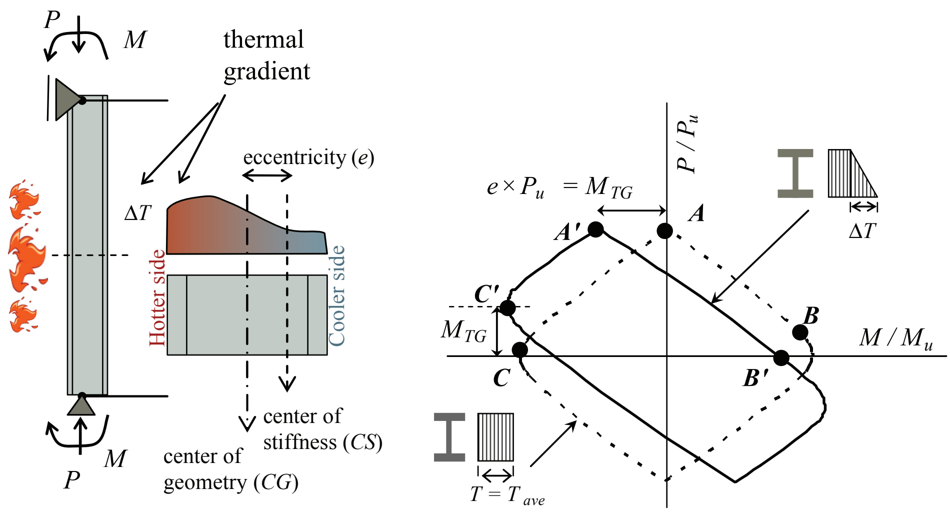

(a) *(b)*

Fig. 3. Characterizing plastic P-M diagram for a W-shape with thermal gradient in the strong direction: (a) development of thermal gradient; (b) effect of thermal gradient on P-M diagrams.

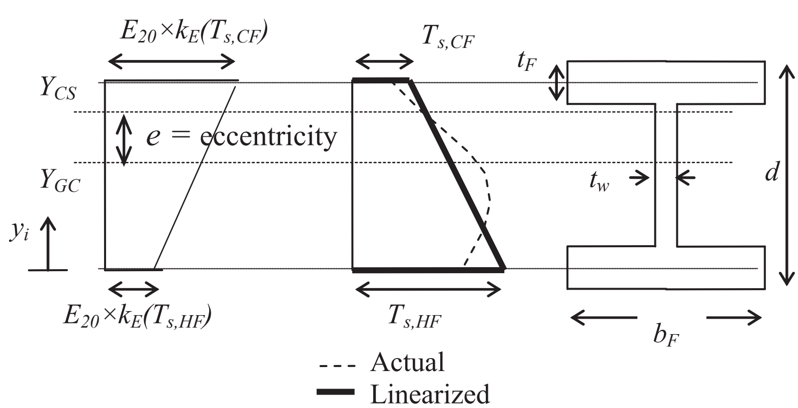

(a) *(b)* *(c)*

Fig. 4. Eccentricity between center of stiffness and center of geometry of a W-shape with thermal gradient: (a) elastic modulus profile; (b) temperature profile; (c) section dimensions.

$$e = \frac{d}{2}\left(\frac{2b_F t_F k_E(T_{s,CF}) + t_w d k_E(T_{s,Ave})}{k_E(T_{s,Ave})(2b_F t_F + t_w d)} - 1\right) \quad (23)$$

where b_F, t_F, t_w and d are dimensions of the section as shown in Figure 4, and $k_E(T)$ is the reduction factor for elastic modulus at steel temperature T.

On the global (member) level, thermal gradient leads to the development of thermal curvature in the beam-column, and this leads to thermal bowing. This is illustrated in Figure 5, which shows the influence of thermal gradient on the local P-Δ effect of the beam-column. Thermal curvature and thermal bowing cause lateral deflection of the beam-column, and this lateral deflection will generate additional P-Δ moment. If we assume a uniform thermal gradient along the length of the beam-column, then thermal curvature will be constant along the beam-column. If the applied end moments on the beam-column are equal and opposite, as shown in Figure 5, then the mechanical curvature due to these bending moments will also be constant. The *elastic* lateral deflection in this case (as shown in Figure 5) can be obtained, according to Mohr's theorem, by integrating the moment of the resultant curvature (thermal minus mechanical curvature) as:

$$\Delta_{TB} = \int_{z=0}^{z=L/2}\left(\alpha\frac{\Delta T}{h} - \frac{M}{E_s(T_{ave})I}\right) z\,dz \quad (24)$$

$$= \left(\alpha\frac{\Delta T}{h} - \frac{M}{E_s(T_{ave})I}\right)\frac{L^2}{8}$$

The increase in bending moment due to thermal bowing can then be evaluated by multiplying the lateral deflection by the axial force in the beam-column:

$$M_{TB} = P \times \Delta_{TB} \quad (25)$$

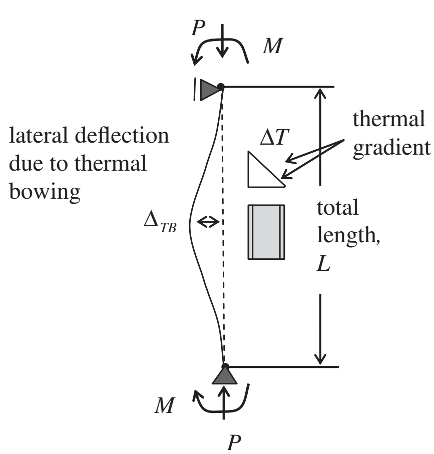

Fig. 5. Influence of thermal gradient on P-Δ effect.

The modification of the P-M interaction curves is based on using the average temperature of steel section with a shift M_{TG} that occurs as a result of thermal gradient in the section, and with second-order effects that arise due to thermal bowing, M_{TB}. The adjustment of P-M diagram is aimed at preserving the room-temperature shape of the P-M diagram and only introducing the shift M_{TG} to account for the thermal gradient effect. The adjusted equations of the plastic P-M diagrams for a wide-flange section with linearized thermal gradient in the strong direction can be written as:

$$\frac{|M + M_{TB} + M_{TG}|}{M_{cr,Tave}} + \frac{P}{P_{cr,Tave}} \le 1.0 \quad (26a)$$

$$\frac{|M + M_{TB} - M_{TG}|}{M_{cr,Tave}} - \frac{P}{P_{cr,Tave}} \le 1.0 \quad (26b)$$

VERIFICATION OF THE PROPOSED APPROACH

The proposed modifications are verified by comparing the predictions against results from nonlinear finite element analysis. In the following section, the nonlinear finite element model for the steel beam-column is introduced, and then the model is validated against data from fire tests. Once the model is validated, it is utilized to verify the proposed modifications as per Equation 26.

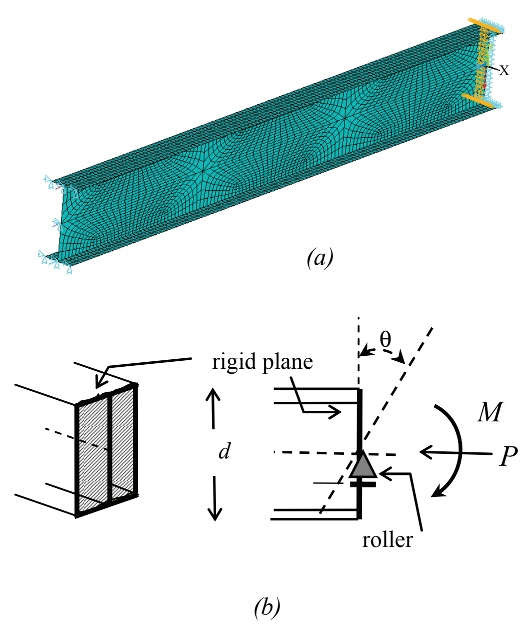

Fig. 6. Structural discretization and modeling of end restraint of beam-column: (a) structural mesh and boundary conditions; (b) model axial and rotational restraints.

Nonlinear Finite Element Analysis

The structural model for the steel beam-column was created using ANSYS (2007). Figure 6a shows the structural mesh and boundary conditions of the beam adopted for the structural analysis. To save on computational expenses, symmetry is utilized, and only half of the beam is modeled. For applying symmetry, in-plane translations and out-of-plane rotations are prevented at the nodes of the midspan section of the beam as shown in Figure 6a. The steel beam is discretized using shell elements (the eight-noded SHELL93 element in ANSYS 2007) that account for material and geometric nonlinearities. Based on sensitivity studies (Dwaikat and Kodur, 2009), the mesh size of the finite elements was chosen to be 30 mm × 30 mm, which means that each plate is modeled with at least three elements of the eight-noded shell element; thus, at least seven nodes were generated across the width of each plate. In the analysis, material nonlinearities include nonlinear temperature-stress-strain curves for steel and temperature-dependent thermal strain. Geometric nonlinearities include large deformations and large rotations. Kinematic constraints are applied on the boundary of the beam-column as shown in Figure 6b. This was to ensure consistent rotation of the end supports conditions according to the applied bending moment.

The high-temperature properties of steel used in the analysis are based on Eurocode properties (EC3, 2005). This is because the temperature-dependent reduction factors for the material properties of structural steel according to AISC specifications are identical to those specified in the Eurocode. Therefore, temperature-stress-strain curves for structural steel according to Eurocode are used for the analysis. The Eurocode coefficient of thermal expansion as a function of steel temperature is also used in the analysis.

Analysis Procedure

Three load steps were applied on the steel beam-column in order to obtain the capacity. In the first step, bending moment *M* is applied gradually on the meshed finite element model of the beam-column. Temperature and thermal gradient along the cross section and over the entire length of the beam-column is applied gradually in the second load step. Finally, in the third step, the axial force *P* is increased until failure occurs in the beam-column. In the numerical analysis, failure is said to occur at the last time step at which convergence is achieved. The maximum sustained axial force and the applied bending moment on the beam-column define a single point on the failure surface (*P-M* diagram) of the beam-column. To obtain another failure point on the *P-M* diagram, the same analysis is repeated but with a different value of initial applied bending moment on the supports. The analysis is also repeated for different span lengths, for average steel temperature and for the case with thermal gradients.

Model Validation

The finite element model is validated by comparing the predictions from analysis with measured data in fire-resistance tests on beam-columns. For this validation, data from fire-resistance tests on steel beam-columns subjected to fire induced thermal gradient are used. The details of the fire resistance test can be found elsewhere (Dwaikat, 2010; Kodur et al., 2009). The tested beam-column—a W8×48 cross section that is 3.3 m (130 in.) in height—was instrumented with thermocouples to measure steel temperatures, strain gauges to measure bending moment, and linear variable differential transformers (LVDTs) to measure displacement and top end rotations. The base of the

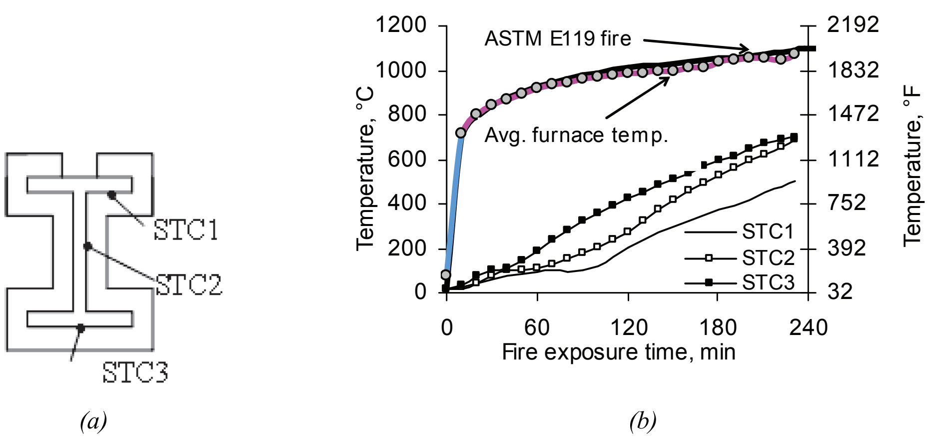

Fig. 7. Recorded steel temperatures in tested beam-column: (a) cross section and thermocouples; (b) fire and steel temperatures.

beam-column was fully fixed using thick steel brackets, while the top end was free to rotate but restrained against lateral translations. The beam-column was subjected to an axial force corresponding to approximately 25% of its room-temperature plastic capacity. The beam-column was exposed to ASTM E119 standard fire (ASTM, 2008) from four sides, and the average insulation thickness was 25 mm (1 in.). In order to generate thermal gradient along the cross section, insulation material was removed from one side, as shown in Figure 7a. The recorded temperatures in the beam-columns in fire-resistance experiments are shown in Figure 7b at the base and at the location of the plastic hinge. The fire-induced axial force and bending moment in the beam-column are plotted in Figure 8 as a function of fire-exposure time.

The base bending moment (shown in Figure 8a) was directly computed using the readings of the strain gauges at the base of the beam-column which remained cool [below 40 °C (104 °F)] during the fire test (Dwaikat, 2010; Kodur et al., 2009). The bending moment at the critical section—where plastic hinge developed at 1930 mm (76 in.) from the base—was interpolated between the moment at the base and zero at the top end. The pressure recorded in the vertical actuators was also used to directly measure the fire-induced axial force. Figure 8 shows that both the axial force and bending moment increase first and then decrease with fire-exposure time. This is because the beam-columns expand nonuniformly under the influence of temperature and thermal gradients until the spread of plasticity in the beam-columns causes a reduction in the axial force.

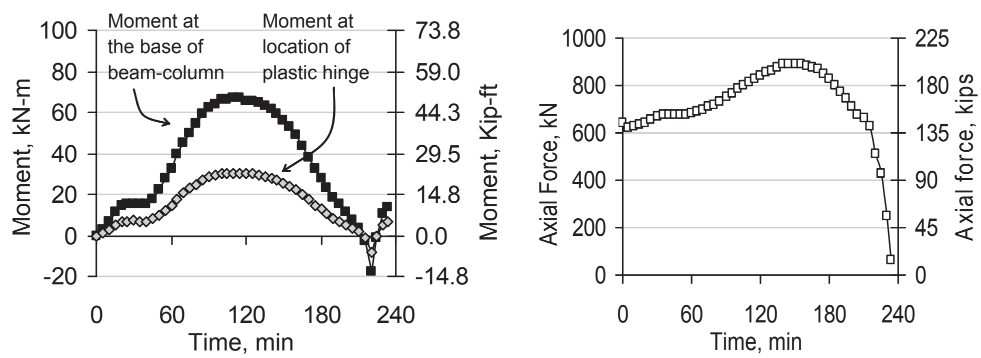

(a) (b)

Fig. 8. Measured fire-induced axial force and bending moment in the tested beam-column: (a) bending moment; (b) fire-induced axial force.

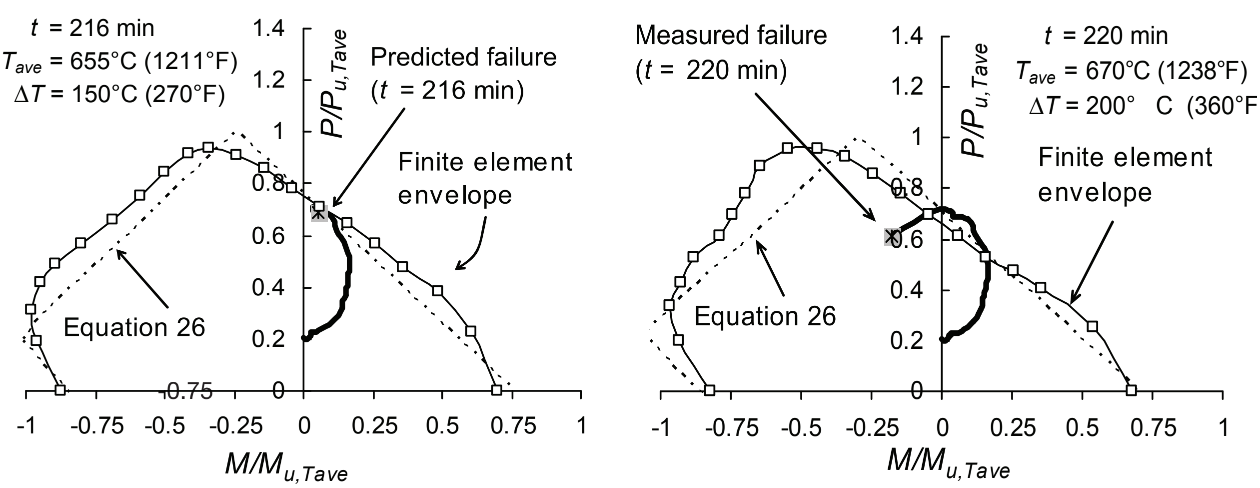

(a) (b)

Fig. 9. Measured and predicted P-M response for the tested beam-column: (a) at t = 216 min of fire exposure; (b) at t = 220 min of fire exposure.

Figure 9 plots the development of the fire-induced P and M in the tested beam-column. The P-M envelope as predicted using finite element analysis and the simplified approach (Equation 26) at two fire-exposure times is also plotted in Figure 9. It is seen in the figure that at different time steps, the beam-column experiences different thermal gradients, which cause different shifts in the P-M diagrams.

Based on the results in Figure 9a, the failure time of the beam-column is conservatively predicted by the detailed finite element analysis at t = 216 min, which matches well with predicted failure envelope using Equation 26. The actual failure of the beam-column was observed in the fire test at t = 220 min, as shown in Figure 9b. The actual failure in test is said to occur at the time after which the beam-column is no longer capable of carrying the applied axial load and thus starts to deflect at an accelerated rate. The predicted failure is assumed to be the time at which the fire-induced P and M exceed the capacity envelope given in Equation 26. The measured failure point is inside the capacity envelope mainly due to the experimental parameters. For instance, the fact that the temperature is not exactly uniform along the length of the beam-column can result in shifting the failure point more conservatively toward the inside of the capacity envelope. The comparison presented in Figure 9 shows that the finite element model is capable of predicting the P-M envelop of beam-columns subjected to thermal gradients.

Comparison with Finite Element Analysis

In order to verify the proposed approach in Equation 26 for predicting P-M diagrams, two steel sections with different cases of thermal gradients are analyzed. Figures 10 and 11 show the comparison between the plastic P-M diagrams for these two sections obtained through nonlinear finite element

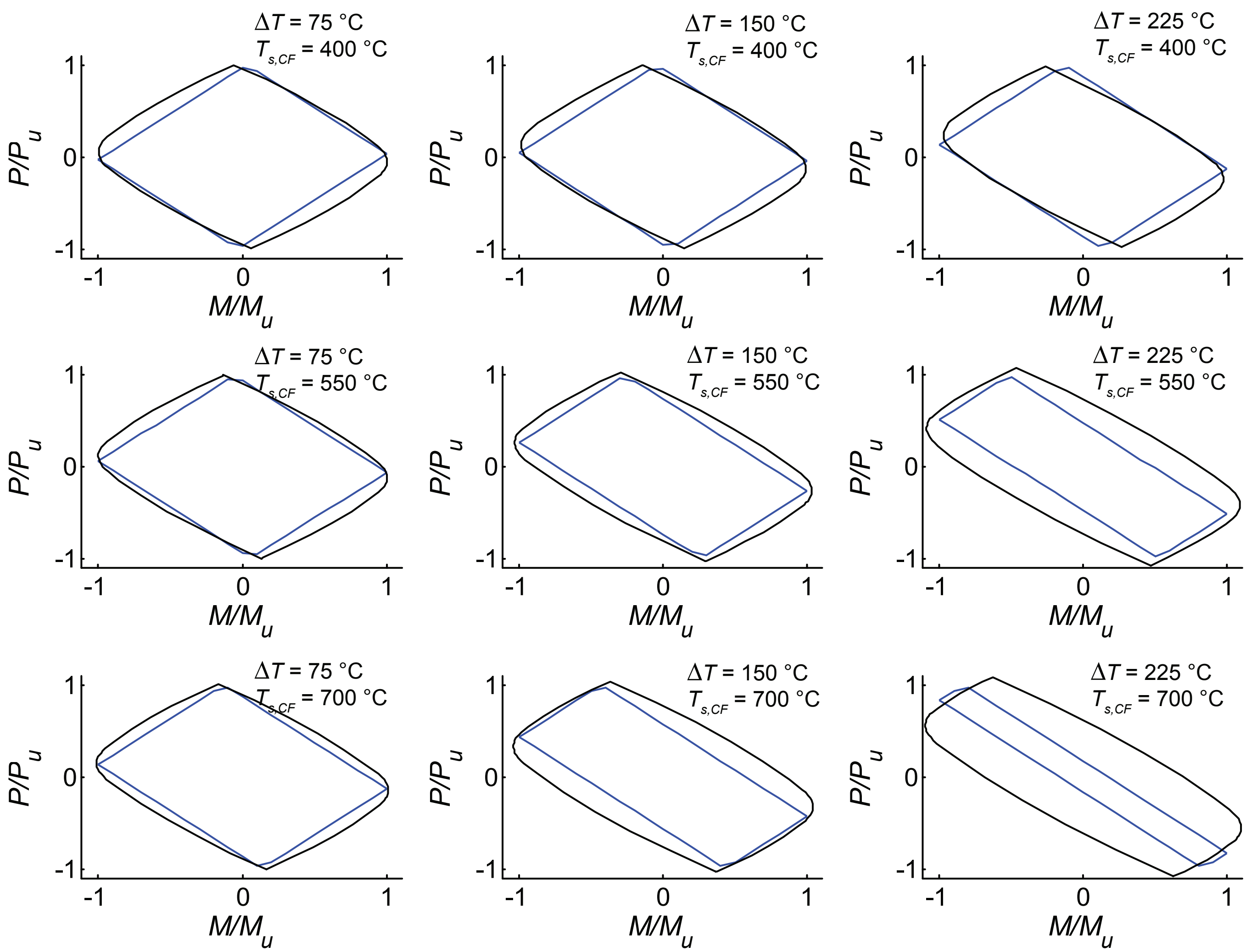

Fig. 10. Plastic P-M diagrams obtained from analysis (solid curves) and as predicted by Equation 26 (dashed curves) for a W24×76 section with different linear thermal gradients along its strong axis ($\Delta T = T_{s,HF} - T_{s,CF}$).

analysis (solid lines) and through the proposed equation (dashed lines). The two sections are W24×76 with relatively thin steel plates and W14×311 with thicker steel plates. These sections were selected to compare the effect of the different steel plate thicknesses on the *P-M* diagrams. The selected sections (W24×76 and W14×311) were subjected to different thermal gradients along their strong axis, and the resulting *P-M* diagrams are normalized to the axial and moment plastic capacities (P_u and M_u) using average temperatures. It can be seen in Figures 10 and 11 that the distortion in the *P-M* diagrams is well predicted using the proposed Equation 26 for both sections. Also, it can be seen in the figures that the distortion is larger for higher temperatures and higher thermal gradients. This is because at higher temperatures [$T_s > 400$ °C (752 °F)], the reduction in steel elastic modulus E_s becomes steeper and thus causes larger eccentricity e between center of stiffness and center of geometry of the nonhomogenous section. Further, the comparisons in Figures 10 and 11 indicate that increasing plate thicknesses has a very small influence on the shape of the *P-M* diagrams under extreme cases of thermal gradients [case $\Delta T = 225$ °C (405 °F)]. It can be seen that Equation 26 conservatively predicts the *P-M* capacity envelopes for realistic cases of thermal gradients.

Figure 12 shows the shape of the *P-M* diagram for beam-columns subjected to thermal gradient and experiencing different types of failure modes. Steel section W18×76 was analyzed for different effective lengths [$KL = 0$, 5 and 10 m (0, 16.4 and 32.8 ft)]. The first case, whose results are presented in Figure 12a, represents plastic failure ($M_{cr} = M_p$ and $P_{cr} = P_y$), while the other cases, as shown in Figures 12b and c, represent inelastic and elastic buckling failure modes ($M_{cr} \leq M_p$ and $P_{cr} \leq P_y$), respectively. Results presented in Figure 12 indicate that the shift in *P-M* diagram

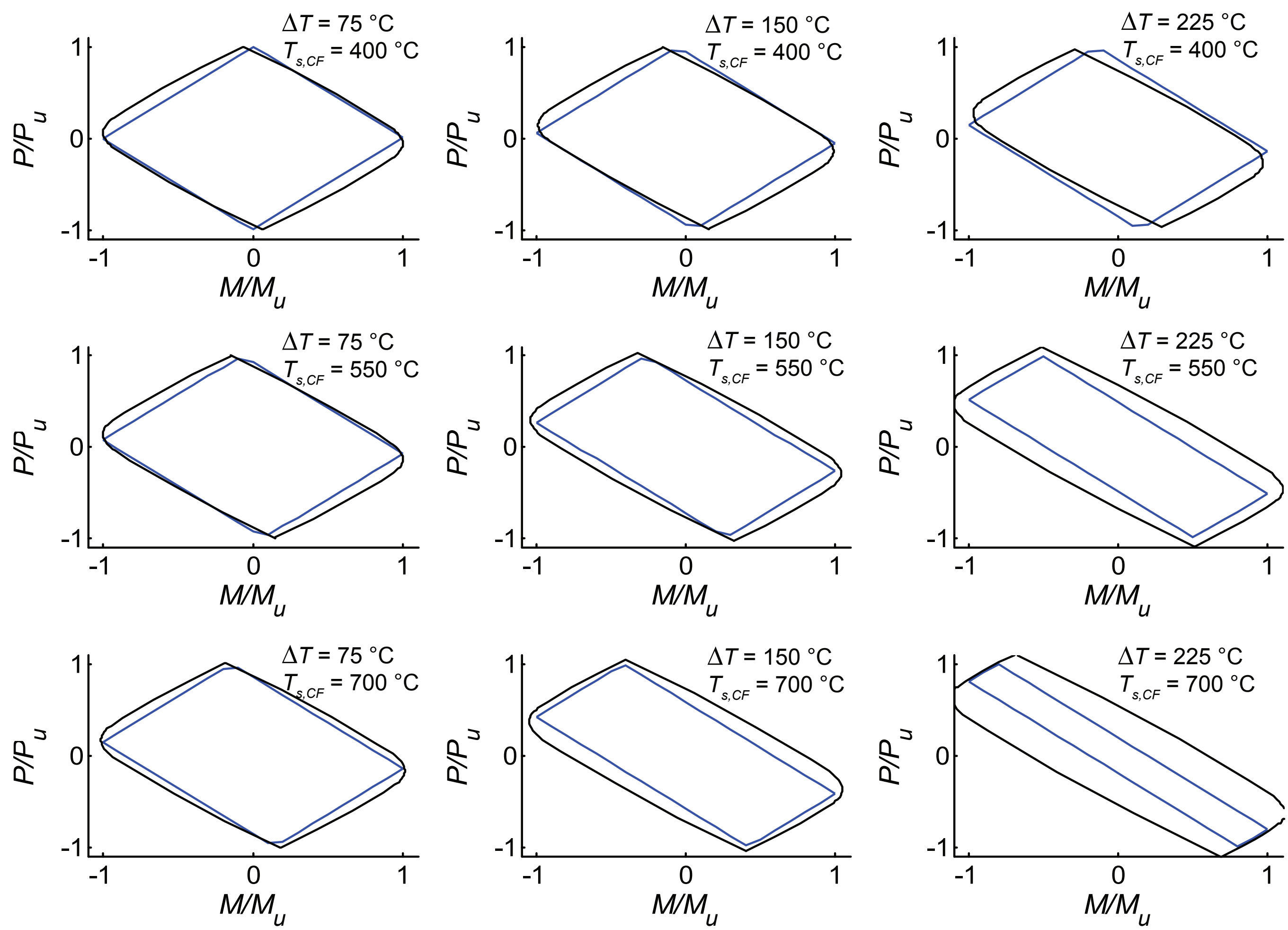

Fig. 11. Plastic P-M diagrams obtained from analysis (solid curves) and as predicted by Equation 26 (dashed curves) for a W14×311 section with different linear thermal gradients along its strong axis ($\Delta T = T_{s,HF} - T_{s,CF}$).

due to thermal bowing (Figures 12b and c) is in the opposite direction as compared to the shift arising due to migration of center of stiffness of the cross section (Figure 12a). This is because the bending moment due to lateral bowing, M_{TB}, and the moment due to thermal gradient, M_{TG}, always occur in an opposite direction to the migration of center of stiffness from the hotter to the cooler side of the cross section. The proposed Equation 26 captures this effect of thermal gradient on the *P-M* capacity envelopes. To date, the *P-M* interaction equations specified in codes and standards do not account for these changes in *P-M* diagrams that arise due to thermal gradient in the beam-column cross section.

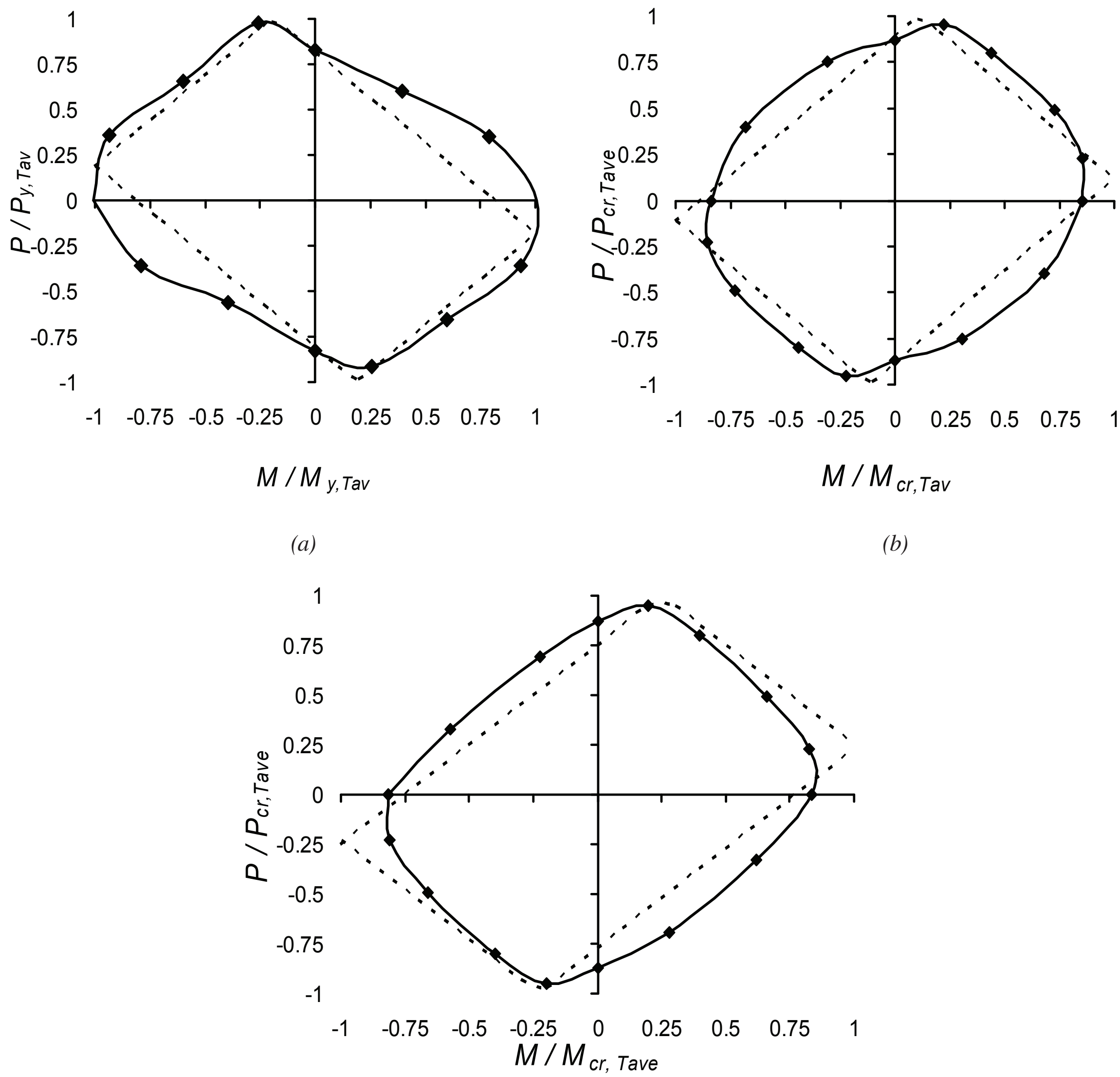

(c)

Fig. 12. P-M diagrams obtained from finite element analysis (solid curves) and as predicted by Equation 26 (dashed curves) for a W18×76 section with linear thermal gradient [ΔT = 200 ºC (360 ºF)] and average temperature of 500 ºC (932 ºF), but different effective lengths: (a) KL = 0 (plastic failure); (b) KL = 5000 mm (16.4 ft) (inelastic failure); (c) KL = 10,000 mm (32.8 ft) (elastic failure).

Table 1. Axial and Moment Critical Capacities According to the AISC, Eurocode, and Takagi and Deierlein Approaches			
Critical Capacities	AISC	Eurocode	T&D
M_{cr} [kN-m (kip-ft)]	1330 (981)	985 (727)	1130 (835)
P_{cr} [kN (kips)]	7150 (1610)	5690 (1280)	4810 (1080)
P_{max} [kN (kips)] using current provisions	3710 (834)	1530 (344)	2090 (470)
Relative error in P_{max} with respect to finite element solution	123%	–7.8%	25.9%
P_{max} [kN (kips)] using Equation 26	1940 (436)	1270 (287)	1780 (401)
P_{max} [kN (kips)] from finite element solution	1660 (374)		

DESIGN EXAMPLE

To demonstrate the applicability of the simplified approach in design situations, a numerical example is presented for a beam-column exposed to ASTM E119 standard fire (ASTM, 2008).

Problem

Assuming the beam-column is braced in the weak direction, compute the maximum compressive force P attained in the beam-column with the following characteristics:

- Beam-column section W14×176 with F_y = 345 MPa (50 ksi)
- Effective and unbraced length of the beam-column is $KL = L_b = 4.5$ m (14.7 ft)
- Average temperature T_{ave} = 500 °C (932 °F), thermal gradient ΔT = 200 °C (360° F)
- Initial bending moment M_o = 320 kN-m (531 kip-ft)

Bending and Axial Capacities

The M_{cr} and P_{cr} for the beam-column described earlier are computed in the strong direction using the three approaches discussed in this paper. The computations are carried out with strength reduction factor ϕ of unity. The results are tabulated in Table 1.

The results in Table 1 show that the *P-M* interaction equations specified in codes and standards overestimate the maximum axial force that can be sustained by the prescribed beam-column. The most nonconservative predictions are using the current AISC *P-M* equations, where the maximum compressive force of 3707 kN (834 kips) was overestimated by more than 123%. The adjustments made by Takagi and Deierlein to the AISC design equation resulted in an improved prediction of 2090 kN (470 kips); however, the maximum axial force that can be carried by the prescribed beam-column is still overestimated by more than 26%, as seen in Table 1. The reason for these nonconservative predictions using *P-M* equations specified in codes and standards is that these equations do not account for the influence of thermal gradient on both stiffness and second-order effect, which greatly affect the capacity of beam-columns.

The Eurocode *P-M* interaction equation provided a reasonable conservative prediction of the maximum compressive force of 1530 kN (344 kips), which was 8% less than the actual compressive force predicted by nonlinear finite element analysis. The reason for improved predictions using the Eurocode is that it uses numerical integration for computing the plastic axial and bending capacities on the sectional level. The numerical sectional integration captures the variation of strength in the cross section arising from the nonuniform thermal gradient.

Table 1 also shows that the predictions of the axial capacity of the beam-column are greatly improved by adopting the modifications proposed in Equation 26 for AISC and T&D equations. This is because these modifications in Equation 26 account for fire-induced thermal gradients by introducing the bending moments M_{TG} and M_{TB} that arise due to the migration of center of stiffness and the thermal bowing in the beam-column, respectively. Applying these modifications to the current Eurocode *P-M* diagrams resulted in further conservatism in the estimation of the axial capacity, P, of the beam-column.

CONCLUSIONS

Based on this study, the following conclusions can be drawn:

1. Current fire design provisions in codes and standards recommend the use of *P-M* based on uniform temperature. These *P-M* diagrams, though adequate for four-sided fire exposure, may not be conservative for beam-columns exposed to fire from one, two or three sides due to fire-induced thermal gradients.
2. A simplified approach is proposed for adjusting the uniform temperature *P-M* curves of an I-shaped cross section to account for the shape distortion, which results due to thermal gradient experienced through one-, two- or three-side fire exposure of beam-columns.
3. The effect of thermal gradient on the *P-M* capacity is twofold. First, thermal gradient causes a migration of center of stiffness of the cross section toward the cooler side. Second, thermal gradient results in a thermal bowing effect, which causes lateral deflection and thus an increase in the P-Δ effect on the beam-column.
4. The proposed method of computing plastic *P-M* diagrams, under thermal gradients, requires minimum computational effort and can easily be incorporated into design situations.

ACKNOWLEDGMENTS

The authors wish to acknowledge the support of the National Institute of Standards and Technology (through Building and Fire Research Laboratory Fire Grant 60NANB7D6120) and the National Science Foundation (through award CMMI 0652292). Any opinions, findings, conclusions, or recommendations expressed in this paper are those of the authors and do not necessarily reflect the views of the sponsors.

REFERENCES

AISC (2005), *Steel Construction Manual*, 13th ed., American Institute of Steel Construction, Chicago, IL.

AISC (2010), *Specification for Structural Steel Buildings*, ANSI/AISC 360-10, American Institute of Steel Construction, Chicago, IL.

ANSYS (2007), *ANSYS Multiphysics Version 11.0 SP1*, ANSYS Inc., Canonsburg, PA.

ASTM (2008), *Standard Methods of Fire Test of Building Construction and Materials: Test Method E119-01*. American Society for Testing and Materials, West Conshohocken, PA.

Burgess, I.W., El-Rimawi, J.A. and Plank, R.J. (1990), "Analysis of Beams with Non-Uniform Temperature Profile Due to Fire Exposure," *Journal of Constructional Steel Research*, Vol. 16, pp. 169–192.

Dwaikat, M.M.S. (2010), "Response of Restrained Steel Beam Subjected to Fire Induced Thermal Gradients," Ph.D. Thesis, Michigan State University, East Lansing, MI.

Dwaikat, M.M.S. and Kodur, V.K.R. (2009), "A Simplified Approach for Evaluating Plastic Axial and Moment Capacity Curves for Beam-Columns with Non-uniform Thermal Gradients," *Engineering Structures*, Vol. 32, pp. 1423–1436.

EC3 (2005). *Eurocode 3: Design of Steel Structures. Part 1-2: General Rules—Structural Fire Design*, EN1993-1-2, European Committee for Standardization, Brussels, Belgium.

Garlock, M.E.M. and Quiel, S.E. (2007), "The Behavior of Steel Perimeter Columns in a High-Rise Building under Fire." *Engineering Journal,* AISC, Vol. 44, No. 4, pp. 359–372.

Garlock, M.E.M. and Quiel, S.E. (2008), "Plastic Axial Load and Moment Interaction Curves for Fire-Exposed Steel Sections with Thermal Gradients," *Journal of Structural Engineering*, ASCE, Vol. 134, No. 6, pp. 874–880.

Kodur, V.R., Garlock, M.E, Dwaikat, M.S. and Quiel, S. (2009), "Collaborative Research: Fire Engineering Guidelines for the Design of Steel Beam-Columns," *Proc. 2009 NSF Engineering Research and Innovation Conference,* Honolulu, HI.

Ma, K.Y. and Liew, J.Y.R. (2004), "Nonlinear Plastic Hinge Analysis of Three-Dimensional Steel Frames in Fire," *Journal of Structural Engineering*, ASCE, Vol. 130, No. 7, pp. 981–990.

Takagi, J. and Deierlein, G.G. (2007), "Strength Design Criteria for Steel Members at Elevated Temperatures," *Journal of Constructional Steel Research*, Vol. 63, pp. 1036–1050.